

Preliminary results on the migration of the tropical rainfall zone in a simple climate model

M. SANKAR-RAO and A. V. KIRAM KUMAR

Department of Aerospace Engineering and Centre for Atmospheric Sciences,
Indian Institute of Sciences, Bangalore 560 012, INDIA

(Manuscript received December 4, 1987; accepted April 18, 1988)

RESUMEN

Dos experimentos numéricos se llevaron a cabo con un modelo climático simple de balance de energía. Uno corresponde a un planeta oceánico y el otro a un planeta de tierra húmeda. Para el planeta de tierra se encontró que el máximo del cinturón de precipitación tropical emigra cerca de 30° en latitud, mientras que para el planeta oceánico, siempre permanece cercano al Ecuador. Debido a la inmovilidad del cinturón de precipitación, en el planeta oceánico se forma un desierto tropical, además del desierto extratropical que surge en los dos experimentos tanto para el planeta terrestre como en el oceánico.

ABSTRACT

Two numerical experiments were performed with a simple energy balance climate model. One is for a global ocean planet and the other one is for a wet land planet. It was found that the tropical rainbelt maximum migrates, for a land planet, about 30° in latitude, while for the ocean planet, it stays always near the equator. Because of this stationarity of the rainbelt in the ocean planet, a tropical desert is formed besides the extratropical desert, which forms both for land and ocean planet experiments.

1. Introduction

One of the interesting features of tropical climatology is the movement of the ITCZ especially over the Indian Region (Sikka and Gadgil, 1980; Webster and Chow, 1980). Webster and Chow, within the framework of a simple model, explained this movement to be related to the land processes. The movement of the ITCZ is not regular (Ramasastry *et al.*, 1986). The purpose of this work is to check if simple toy climate models can be used for a further understanding of this type of climatological phenomenon with a time scale of a month or larger.

2. Model and methodology

2.1 Master equations

We followed closely Sellers (1973) and Saltzman and Vernekar (1971) to construct our model for two reasons: first we had the guidance of former results and second, we checked what those models clarify. We started with Saltzman and Vernekar's (1971) equations for the vertically integrated potential temperature and the mixing ratio of the atmosphere.

$$\frac{\partial \bar{\theta}_{o_a}}{\partial t} = -\frac{\delta_1}{a \cos \phi} \frac{\partial}{\partial \phi} (\bar{v}_{o_a} \bar{\theta}_{o_a} \cos \phi) + \frac{\delta_2}{a \cos \phi} \frac{\partial}{\partial \phi} \frac{K_{HT}}{a} \frac{\partial \bar{\theta}_{o_a}}{\partial \phi} + \delta_3 \left(\frac{p_s}{p_a} \right)^{\mathcal{R}} \bar{Q}_{o_a}^{(n)} \quad (1)$$

$$\begin{aligned} \frac{\partial \bar{\bar{\epsilon}}_{o_a}}{\partial t} = & -\frac{\delta_4}{a \cos \phi} \frac{\partial}{\partial \phi} (\bar{v}_{o_a} \bar{\bar{\epsilon}}_{o_a} \cos \phi) \\ & + \frac{\delta_5}{a \cos \phi} \frac{\partial}{\partial \phi} \frac{K_{H\epsilon}}{a} \frac{\partial \bar{\bar{\epsilon}}_{o_a}}{\partial \phi} - \delta_6 \left(\frac{1}{L} \theta_{o_a}^{(4)} + \frac{g}{p_s} \frac{1}{L} H_{o_s}^{(4)} \right). \end{aligned} \quad (2)$$

The notation is given in the Appendix. However, for convenience, we explain a few symbols in the text. Here the suffix a stand for the atmosphere, S for the surface, 0 for the zonal mean and the double bar indicates zonal and vertical average; δ_i are indices that take value 0 or 1 and are introduced to keep or drop the term.

The model atmosphere has a prescribed vertical structure as given below:

$$v_{o_a}(p) = v_{o_s} \left(\frac{2p - p_s}{p_s} \right) \quad (3)$$

$$\omega_{o_a}(p) = -\frac{p(p - p_s)}{p_s} \frac{1}{a \cos \phi} \frac{\partial}{\partial \phi} (v_{o_s} \cos \phi) \quad (4)$$

$$\epsilon_{o_a}(p) = \epsilon_{o_s} (p/p_s)^\xi \quad (5)$$

$$\theta_{o_a}(p) = \theta_{o_a} + (p - p_a) \left(\frac{\theta_{o_s} - \theta_{o_a}}{p_s - p_a} \right). \quad (6)$$

Eqs. (3) and (4) satisfy the continuity equation with the boundary condition $\omega = 0$ at $p = p_s$ and $p = 0$.

In (1) $Q_{o_a}^{(n)}$ are the various atmospheric components of heating:

$Q_{o_a}^{(1)}$: heating due to short wave radiation

$Q_{o_a}^{(2)}$: heating due to long wave radiation

$Q_{o_a}^{(3)}$: heating due to sensible heat

$Q_{o_a}^{(4)}$: heating due to condensation.

After substituting (3) and (4) in (1) and (2), and integrating with respect to p we can write from (3):

$$\begin{aligned} \frac{\partial \theta_{o_a}}{\partial t} = & \frac{\delta_1}{3} \frac{1}{a \cos \phi} \frac{\partial}{\partial \phi} (v_{o_s} \theta_{o_a} - v_{o_s} \theta_{o_s}) \cos \phi \\ & + \frac{\delta_2}{a \cos \phi} \frac{\partial}{\partial \phi} K_{TH} \frac{1}{a} \frac{\partial \theta_{o_a}}{\partial \phi} + \frac{\delta_3}{p_s} \left(\frac{p_s}{p_a} \right) \Re \left[\frac{g}{c_p} (H_{o_a}^{(1)} + H_{o_a}^{(2)} + H_{o_a}^{(3)}) + \frac{Q_{o_a}^{(4)}}{L} \right], \end{aligned} \quad (7)$$

where $H_{o_a}^{(n)}$ represents net flux across the upper and lower surfaces. From (4) we get

$$\begin{aligned} \frac{\partial \epsilon_{o_s}}{\partial t} = (1 + \xi) & \left[-\frac{\delta_4 \xi}{(\xi + 1)(\xi + 2)} \frac{1}{\text{acos}\phi} \frac{\partial}{\partial \phi} (\epsilon_{o_s} v_{o_s} \cos\phi) \right. \\ & \left. + \frac{\delta_5}{(\xi + 1)} \frac{1}{\text{acos}\phi} \frac{\partial}{\partial \phi} \frac{K_{H\epsilon}}{a} \frac{\partial \epsilon_{o_s}}{\partial \phi} + \frac{\delta_6 g}{L p_s} (-H_{o_s}^{(4)} - \frac{p_s}{g} \frac{1}{L} Q_{o_s}^{(4)}) \right]. \end{aligned} \quad (8)$$

Eqs.(7) and (8) are the master equations for the atmospheric part of the energy balance model. Similar to (1) and (2) the lower fluid surface equation is written as:

$$\frac{\partial \bar{\theta}_{ow}}{\partial t} = -\frac{\delta_7}{\text{acos}\phi} \frac{\partial}{\partial \phi} (\bar{v}_{ow} \bar{\theta}_{ow} \cos\phi) + \frac{\delta_8}{\text{acos}\phi} \frac{\partial}{\partial \phi} \frac{K_{Hw}}{a} \frac{\partial \bar{\theta}_{ow}}{\partial \phi} + \frac{\delta_9}{C_s M} H_{o_s}^{(n)} \quad (9)$$

for solid lower surface $\delta_7 = \delta_8 = 0$. Following Sellers (1973) if we assume a vertical structure for the ocean and write

$$\theta_{ow} = \theta_D + (\theta_{os} - \theta_D) e^{\bar{a}z} \quad (10)$$

$$v_{ow} = v_{ows} e^{\bar{a}z} (1 + \bar{a}z) \quad (11)$$

$$v_{ows} = -10^{-2} u_{os} \quad \text{in the Northern Hemisphere} \quad (12)$$

$$v_{ows} = +10^{-2} u_{os} \quad \text{in the Southern Hemisphere.} \quad (13)$$

Using (10) to (13) we can integrate (9) in the vertical coordinate and write

$$\begin{aligned} \frac{\partial \theta_{os}}{\partial t} = & \left\{ -\frac{\delta_7}{\text{acos}\phi} \frac{\partial}{\partial \phi} [\theta_D v_{ows} e^{\bar{a}h} + (\theta_{os} - \theta_D) v_{ows} \left(\frac{1 - e^{-2\bar{a}h}}{4\bar{a}h} + \frac{e^{-2\bar{a}h}}{2} \right) \cos\phi] \right. \\ & + \frac{\delta_8}{\text{acos}\phi} \frac{\partial}{\partial \phi} \frac{K_{Hw}}{a} \frac{\partial}{\partial \phi} \left[\frac{\theta_{os}(1 - e^{-\bar{a}h})}{\bar{a}h} + \theta_D \left(1 - \frac{1 - e^{-\bar{a}h}}{\bar{a}h} \right) \right] \\ & \left. + \frac{\delta_9}{C_s M} H_{o_s}^{(n)} \right\} \left(\frac{1 - e^{-\bar{a}h}}{\bar{a}h} \right)^{-1}. \end{aligned} \quad (14)$$

In the above equations for the surface:

z : depth measured negative from the surface

θ_D : subsurface temperature

$$\bar{a} = \frac{\pi}{h_w}$$

h_w : depth of the active layer.

Eqs. (7), (8) and (14) constitute the set for the atmosphere and the lower surface. Now that we have written down the master set of equations we shall turn to the fluxes appearing in them.

2.2 Heat fluxes

For the heat fluxes we follow Saltzman and Vernekar (1971) and write them as follows:

$$H_{oa}^{(1)} = \chi(1 - \lambda_a)R_o \quad (15)$$

$$\begin{aligned} H_{oa}^{(2)} &= \sigma[\Gamma T_s^4 - (\nu_1 + \nu_2)T_a^4] \\ &= \sigma[\Gamma \theta_{os}^4 - (\nu_1 + \nu_2)\left(\frac{p}{p_s}\right)^{4\beta} \theta_{oa}^4] \end{aligned} \quad (16)$$

$$H_{oa}^{(3)} = b_2(\theta_{os} - \left(\frac{p}{p_s}\right)^{\beta} \theta_{oa}) + C_2 \quad (17)$$

$$Q_{oa}^{(4)} = \frac{Lg}{p_s} R_f = \frac{Lg}{p_s} (R_{f_1} + R_{f_2}). \quad (18)$$

Here R_f is the rainfall, R_{f_1} is the large scale rainfall and R_{f_2} is the cumulus scale rainfall. We compute R_{f_1} and R_{f_2} by

$$R_{f_1} = \frac{0.5}{g} \int_0^{p_s} [\epsilon_o(p) - \epsilon_o^*(p)] dp \quad \text{for } \omega_{os} < 0 \quad (19)$$

$$R_{f_2} = \frac{C_p}{Lg} \int_0^{p_s} \Phi dp \quad (20)$$

$$\Phi = -\left(\frac{\omega_o(p)}{\omega_o(p_a)} \frac{\epsilon_{oa}}{\epsilon_{os}^*} \omega_{oB}\right) \frac{\partial \theta_{oa}}{\partial p} \bar{w} \quad \text{for } \omega_{oB} < 0 \quad (21)$$

$$\Phi = 0 \quad \text{for } \omega_{oB} > 0. \quad (22)$$

Eq. (19) condenses 50% of excess moisture above saturation, to fall as rain. While (20) gives convective rain when there is upward vertical velocity. R_{f_2} was considered only in tropics. Outside the tropics it was neglected. Now we define the surface fluxes.

$$H_{os}^{(4)} = \bar{w}(e_2 H_{os}^{(3)} + f_2) = \bar{w}(-e_2 H_{oa}^{(3)} + f_2) \quad (23)$$

$$H_{os}^{(1)} = (1 - \chi)(1 - \lambda_a)(1 - \lambda_s)R_o \quad (24)$$

$$H_{os}^{(2)} = \sigma[\nu_1 \left(\frac{p}{p_s}\right)^{4\beta} \theta_{oa}^4 - \Gamma \theta_{os}^4] \quad (25)$$

$$H_{os}^{(3)} = -H_{oa}^{(3)} \quad (26)$$

$$H_{os}^{(5)} = -\bar{\chi}(\theta_{os} - \theta_D). \quad (27)$$

Eqs. (15) to (27) define the forcing fluxes and the rainfall. These constitute the diabatic forcings for the atmosphere and for the lower surface.

2.3 Feed-backs

The cloud effect on the short wave radiation is simply parameterized as

$$S_{on} = S_o(1 - a_1 n), \quad (28)$$

where n is the cloud amount, S_{on} is the incoming radiation for cloudy skies and S_o is for clear skies.

For long wave radiation we followed Kondratyev (1972) and wrote

$$G_{on} = G_o(1 + C'_1 n),$$

$$C'_1 = C_o \left(\frac{B_o}{G_o} - 1 \right), \quad (29)$$

here:

G_{on} : downward long wave radiation for cloud amount n

G_o : downward long wave radiation for clear skies

B_o : upward long wave radiation for clear skies from the surface.

Hence in our notation

$$G_o = \nu_1 \sigma \left(\frac{p}{p_s} \right)^{4.9R} \theta_{oa}^4 \quad (30)$$

$$B_o = \Gamma \sigma \theta_{os}^4. \quad (31)$$

The cloud amount n is determined in the model by considering precipitation. At points of maximum precipitation on the globe ($R_{f\max}$), the cloud amount is given by a value of 0.5. So we define n by

$$n = 0.5 \frac{R_f}{R_{f\max}}. \quad (32)$$

For water availability we have taken

$$\bar{w} = 1 \quad \text{for ocean} \quad (33)$$

$$\bar{w} = 0 \quad \text{for ice} \quad (34)$$

$$\bar{w} = \frac{S_m}{H_d P^o} \quad \text{for land; } \bar{w} \leq 1 \quad \text{if } S_m > H_d P^o. \quad (35)$$

For land, S_m is calculated at any time step as:

$$S_m = S_m + (R_f - ev)$$

in which R_f is rainfall and ev is evaporation.

In (35) S_m is soil moisture, P^o porosity and H_d active depth. According to (35) $\bar{w} = 0$ if $S_m = 0$ and $w = 1$ if $S_m = P^o H_d$.

For density of the surface we took:

ρ_{si} : density of ice

ρ_{sw} : density of ocean waters.

Density of the wet soil:

$$\rho_{sws} = \frac{1}{1+e}(\rho_s D_s + e\rho_w \bar{w}). \quad (36)$$

In (36) $\rho_s D_s$ is the density of the dry soil and e the void ratio. For the specific heat of the surface we adopted:

Specific heat of ice: $C_{si} = 2.0 \times 10^3$ Joules/kg/ o K

Specific heat of ocean waters: $C_{sw} = 4.2 \times 10^3$ Joules/kg/ o K

Specific heat of wet soil:

$$C_{sws} = \frac{[C_s D_s + \frac{\rho_{sws}}{\rho_s D_s} e \bar{w} C_{sw}]}{[1 + \frac{\rho_{sw}}{\rho_s D_s} e \bar{w}]} \quad (37)$$

In (37) $C_s D_s$ is the specific heat of the dry soil.

For surface albedo we took:

Albedo of surface ice: $\lambda_{si} = 0.5$

Albedo of surface ocean waters: $\lambda_{sw} = 0.06$

Albedo of wet soil:

$$\lambda_{sws} = \lambda_s D_s (1 - \bar{w}) + \lambda_{sw} \bar{w}. \quad (38)$$

In (38) $\lambda_s D_s$ is albedo of dry soil.

For the ice cover we assumed that the surface temperature determines the ice line (Budyko, 1961). The threshold temperature is taken as 263^o K. If the surface temperature falls below 263^o K there will be ice. Otherwise it will be the underlying surface. This type of ice albedo feed-back is admittedly too simple; however, as a first step it can be adequate.

2.4 Closure

To connect ν_{os} and θ_{os} we follow Sellers (1973) and write

$$f \nu_{os} - \bar{a}_* u_{os} | u_{os} | = 0 \quad (39)$$

$$f u_{os} + \bar{a}_* \nu_{os} | \nu_{os} | + R_d (1 - b) \frac{\partial \theta_{os}}{\partial y} = 0. \quad (40)$$

The purely empirical parameter b , given by Sellers (1973) is used here. Fixing b is like fixing the geographical location of the Ferrel cell in Sellers parameterization. In the future it may be better to modify this part by introducing momentum considerations (Saltzman and Vernekar, 1971; Held and Hou, 1980).

3. Methodology of solution and some experiences

Numerical methods are the most suitable tool to solve the above complicated system. We used the well known upwind differencing explicit method. We took 5° in latitude as the interval grid. From pole to pole the grid has 37 points. We ran many preliminary experiments without advection and diffusion and found that the model gives results which are comparable to those of Sellers (1973), Saltzman and Vernekar (1971), Kurihara (1971) and Kubota (1972). Once we introduced the advection and diffusion we found that poles can cause numerical problems unless we give consistent and correct lateral boundary conditions. We used a 6 hour time step in all calculations. When we tried to run an experiment with a completely dry land planet, computational instability developed even with 1 hour time step because the land gets hotter, winds become very strong and the CFL criterion is violated quite soon. We think that some amount of soil moisture is necessary to run land planet experiments if we have limited resources.

We describe here two experiments and their results. One is for ocean globe and the other one for wet land globe.

4. Experiments and the results

4.1 Ocean planet experiment

This experiment was run for a global swamp ocean ($\delta_7 = \delta_8 = 0$).

The initial conditions for this experiment are:

- (a) A global ocean.
- (b) Ice ($h_i = 20$ m) from 70° to the poles.
- (c) θ_{os} and θ_{oa} , temperatures which are close to the present day ones.

With these initial conditions we first obtained a convergent solution with the Sun fixed at equinox (March 21). To get an equinox convergent solution to an accuracy of 0.01°K in temperature everywhere takes nearly four years of integration.

This equinoxial convergent solution is our starting point. We introduced the annual displacement of the Sun from now and integrated in time. There arise a number of questions here. How long should we integrate? Does the atmosphere repeat its state year after year after some time to a prescribed accuracy? Do the daily values repeat? Or do the time means, say monthly means or weakly means, repeat? If they do not repeat, what is the interannual variability like? etc. We decided to look at monthly mean temperatures, by integrating until we got the values repeated at every grid point to an accuracy of 0.05°C . This ocean experiment was integrated for nine years to attain such an accuracy with the equinoxial convergent field initial conditions.

In Figs. 1, 2 and 3 we give the surface monthly mean temperature history. The first month is from March 21 to April 21. The second month is from April 21 to May 21 and so on. We notice the following in these figures.

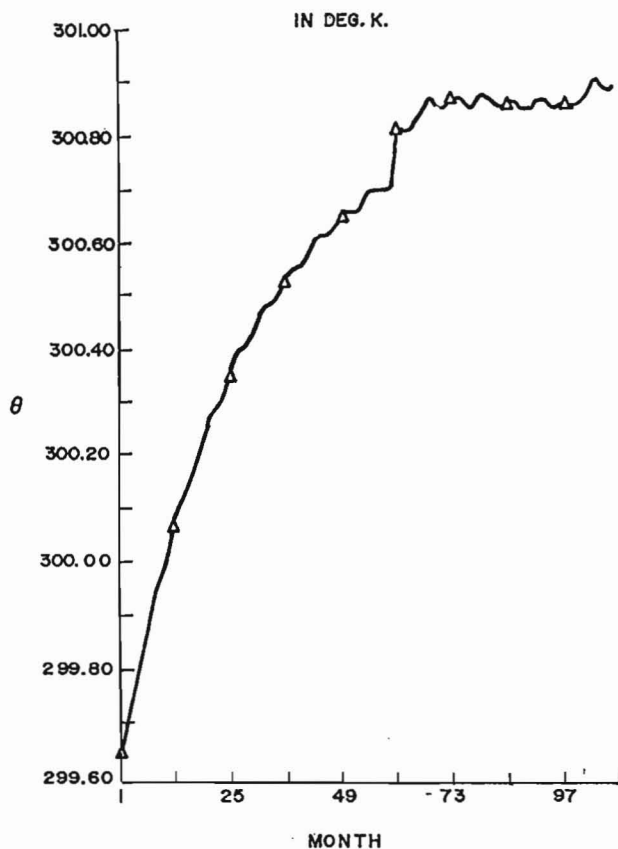


FIG. 1. VARIATION OF SURFACE POTENTIAL TEMPERATURE AT THE EQUATOR WITH TIME (O.P)

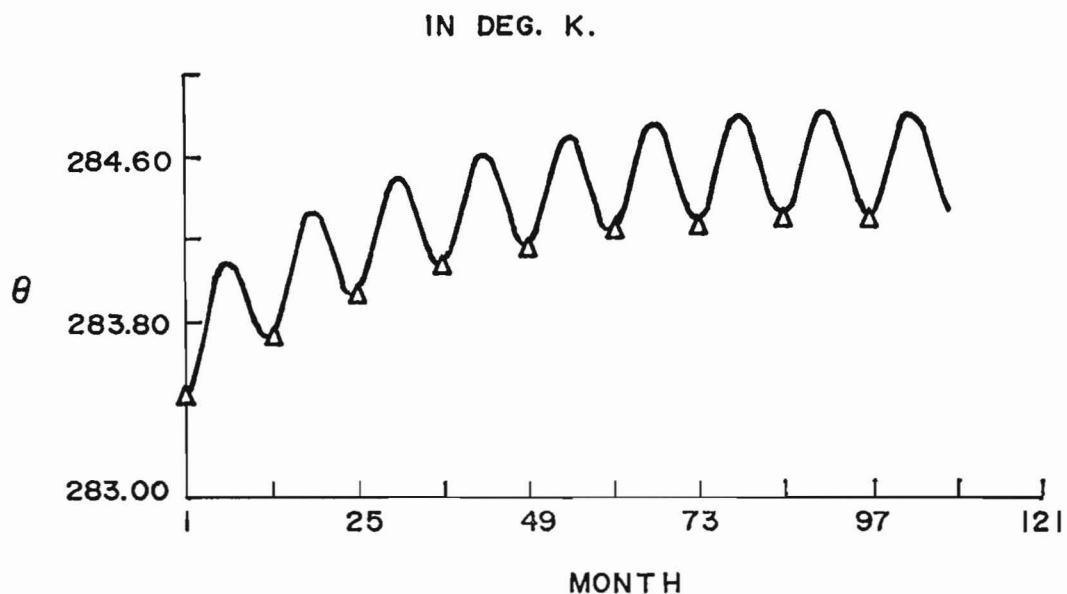


FIG. 2. VARIATION OF SURFACE POTENTIAL TEMPERATURE AT 45° WITH TIME (O.P)

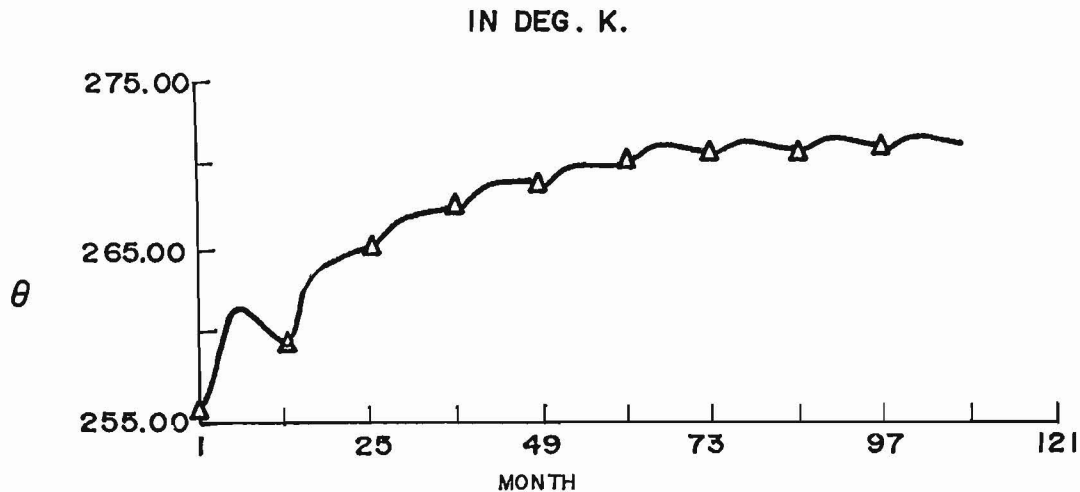


FIG. 3. VARIATION OF SURFACE POTENTIAL TEMPERATURE AT NORTH POLE WITH TIME.(O.P)

(a) It took nearly six years for the surface temperature at the equator to get a state with interannual variability of about 0.05°C .

(b) One can notice the semiannual cycle at the equator, and annual cycles at 45°N and at the pole.

(c) At the pole, the temperatures increased gradually and within two years they are above 263°K . Final temperatures are about 272°K . Thus complete deglaciation took place.

(d) Once the ice melted at the poles it never got recovered. The ice physics parameterization in this model is too simple. These results depend on the threshold temperature of 263°K .

In Figs. 4 to 9 we give atmospheric potential temperature (θ_{0a}) and Rainfall (R_f) profiles for the months of March, July and January, of the 9th year. We notice the following:

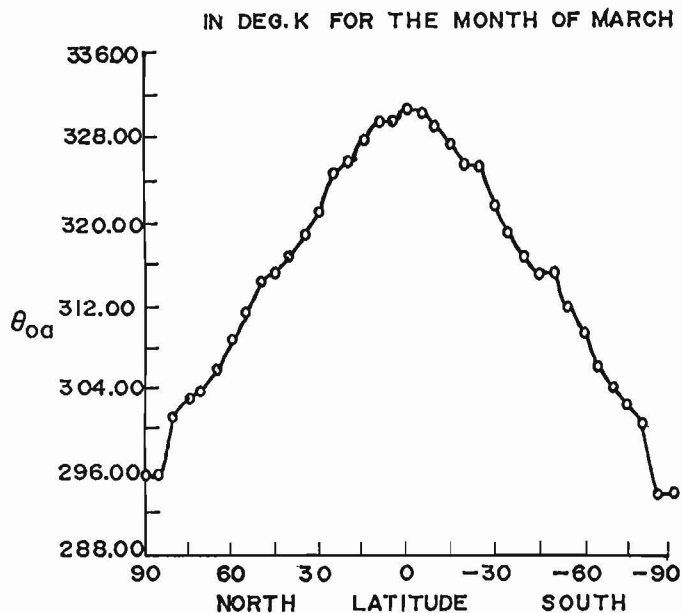


FIG. 4 .VARIATION OF ATMOSPHERIC POTENTIAL TEMPERATURE' WITH LATITUDE(O.P)

(a) The potential temperature difference during summer and winter between the poles is about 27°C .

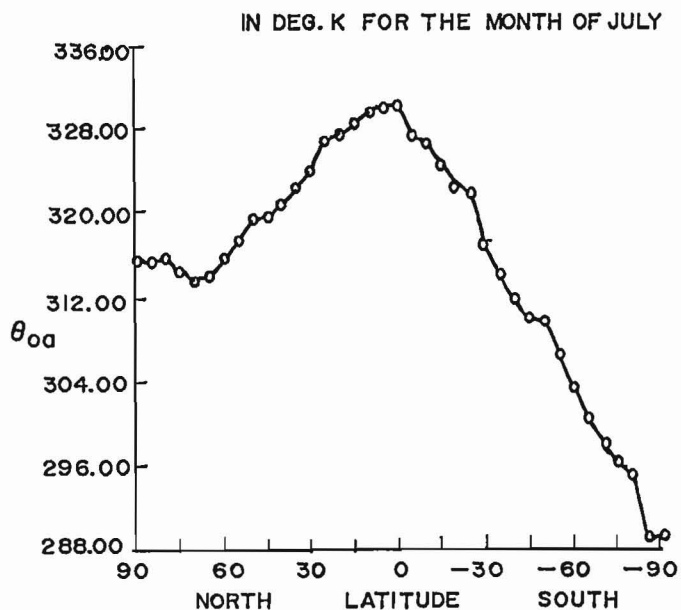


FIG. 5 VARIATION OF ATMOSPHERIC POTENTIAL TEMPERATURE WITH LATITUDE (O.P)

(b) Steepest temperature gradients occur in the winter hemisphere in which the potential temperature difference between the pole and the equator is about 41°C .

(c) Maximum rainfall always occurs near the equator.

(d) In the middle latitudes, the rainfall is more during winter.

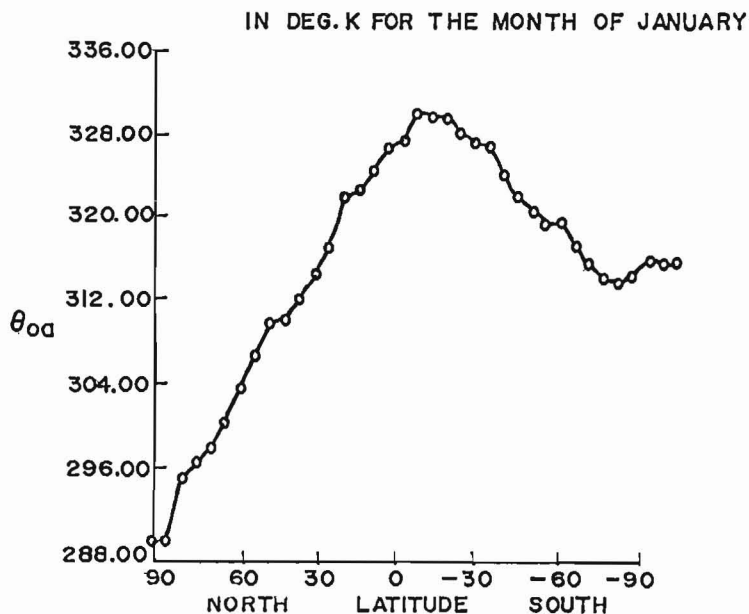


FIG. 6 VARIATION OF ATMOSPHERIC POTENTIAL TEMPERATURE WITH LATITUDE (O.P)

(e) The maximum rainfall zone shifts very little from one season to other (less than 5° in latitude) in this global ocean experiment.

(f) A tropical desert between latitudes 10° and 20° and an extra tropical desert between 30° to 45° in both the hemispheres formed in the experiment. Such results depend on closure assumptions between u_{os} and v_{os} and θ_{os} . Ocean currents can also alter these results. We must, in future, introduce momentum considerations for closure and also the ocean currents and study the differences.

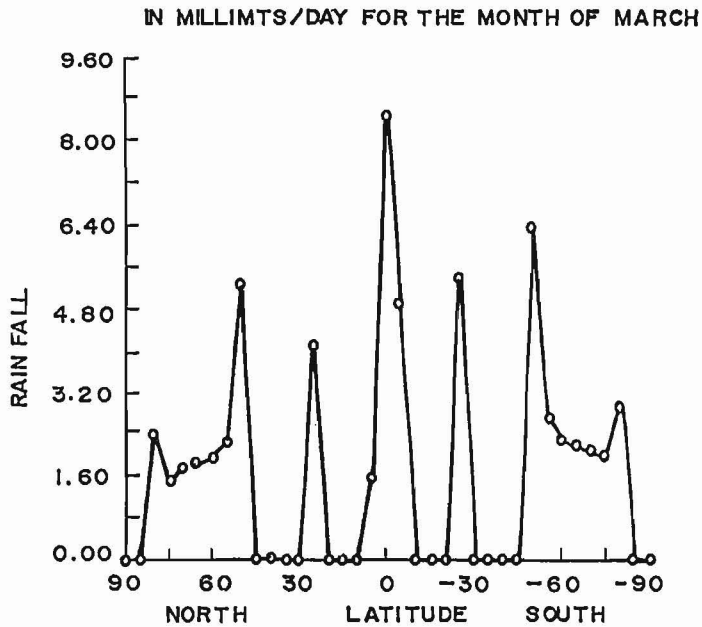


FIG. 7 .VARIATION OF RAIN FALL WITH LATITUDE (O.P)

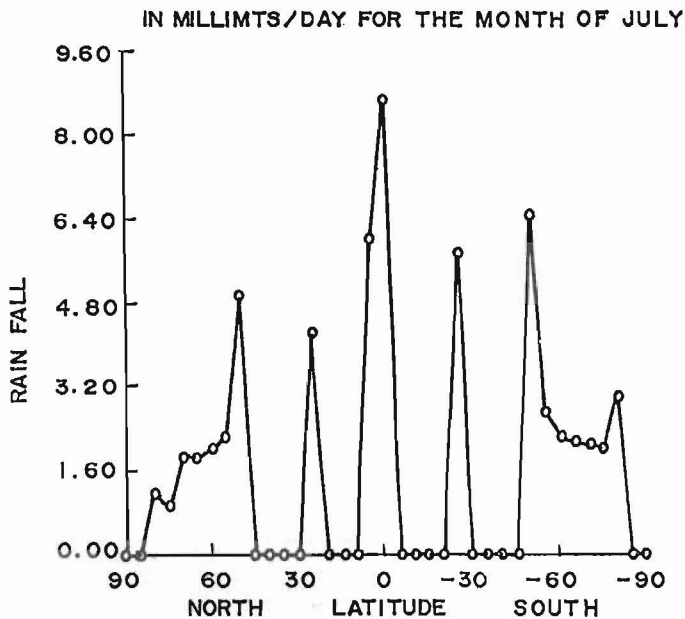


FIG. 8 VARIATION OF RAIN FALL WITH LATITUDE (O.P)

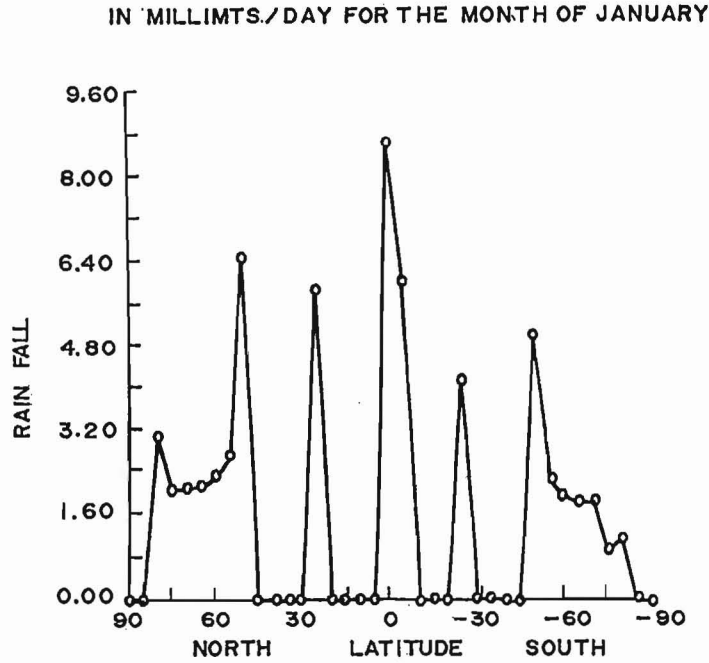


FIG. 9 VARIATION OF RAIN FALL WITH LATITUDE (O.P)

4.2 Land planet experiment

In this experiment we took initially the following conditions:

- (a) Dark soil with 500 mms of soil moisture everywhere.
- (b) 20 meters of ice from 70° to the poles.
- (c) Temperatures which are close to the present day ones.

Just as in the ocean planet experiment we first obtain equinoxial convergent solution with these conditions and then introduce the displacement of the Sun. We observed the following:

- (a) The middle latitudes soil became completely dry when we got the equinoxial convergent solution.

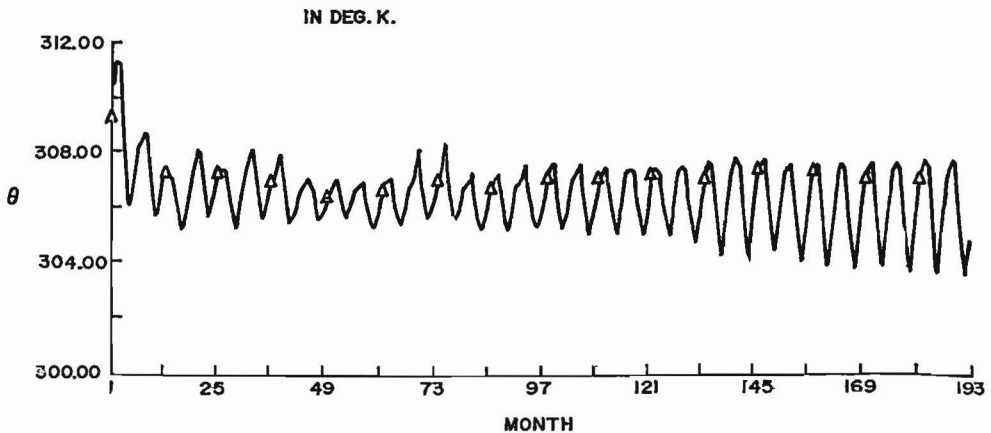


FIG.10: VARIATION OF SURFACE POTENTIAL TEMPERATURE AT EQUATOR WITH TIME (L.P)

(b) At the polar and at the equatorial regions the soil moisture rose from an initial value of 500 mm to a higher one of 2500 mm. Thus the middle latitudes soil moisture was dumped both at the polar and equatorial regions because of the symmetry in the hemispheric poloidal cells.

(c) As in the ocean experiment, the model gives a desert in the middle latitudes, for the initial equinoxial equilibrium solution.

In Figs. 10, 11 and 12 we give the surface temperature history for the equator, 45°N and the North Pole. We notice the following:

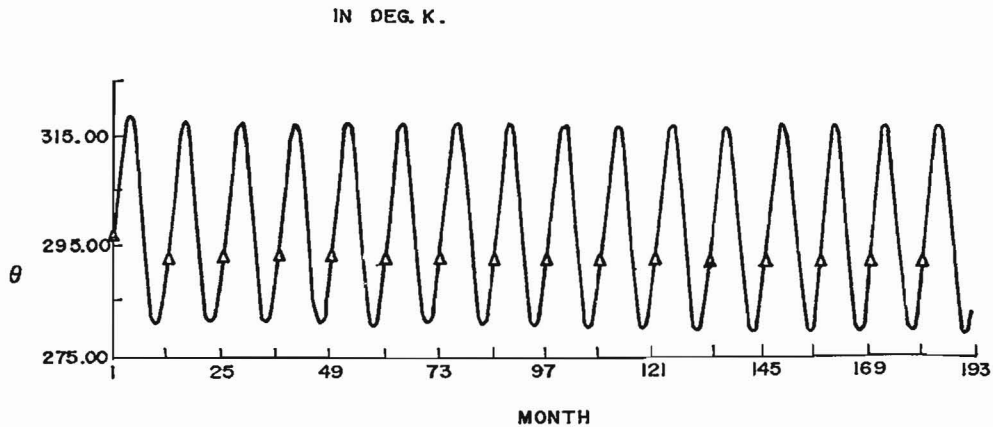


FIG.11. VARIATION OF SURFACE POTENTIAL TEMPERATURE AT 45° WITH TIME (L.P)

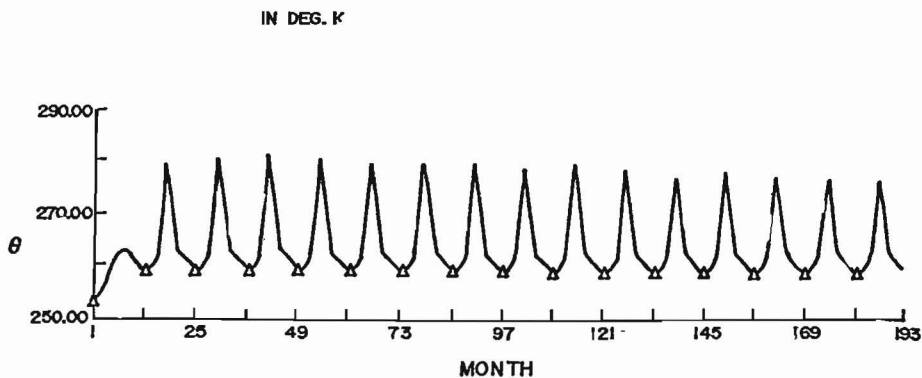


FIG.12. VARIATION OF SURFACE POTENTIAL TEMPERATURE AT NORTH POLE WITH TIME (L P)

(a) After nearly 13 years of integration, the surface temperatures at the equator seem to have reached a repetitive convergent solution.

(b) The amplitude of the seasonal cycle is increased after 12 to 13 years. We find that this is also due to a gradual drying up of the equatorial regions.

In Fig. 13 is shown the soil moisture history at the equator. We note that the equatorial soil moisture dropped from nearly 2600 mm, to about 200 mm in about 10 years and stabilized there. Thus the transport loss is about 240 mm per year. Did such things happen in the early stages of the ocean formation? Did the water accumulate in the oceans much faster than 250 mm per year in the past? These are some of the fascinating questions for which we must seek answers in the future.

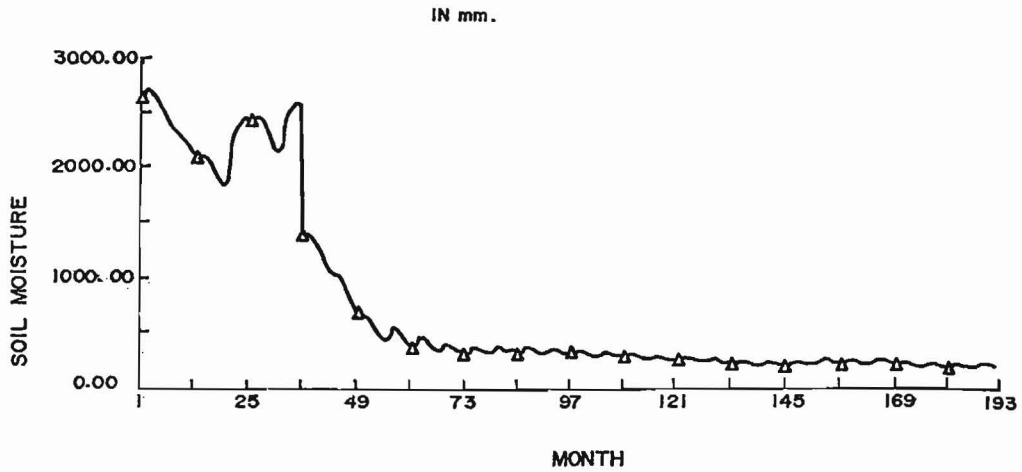


FIG. 13 VARIATION OF SOIL MOISTURE AT THE EQUATOR WITH TIME (L.P)

In Figs. 14 to 19 we show θ_{0a} and R_f profiles for the months of March, July and January of the 16th year. We notice the following:

(a) The potential temperature difference between the poles during summer and winter is about 52°C . This is almost the double that the one obtained for the ocean globe.

(b) The temperature difference between the equator and the winter pole is also about 50°C . Thus at 500 mb level, equator is only slightly warmer than the summer pole.

IN DEG.K FOR THE MONTH OF MARCH

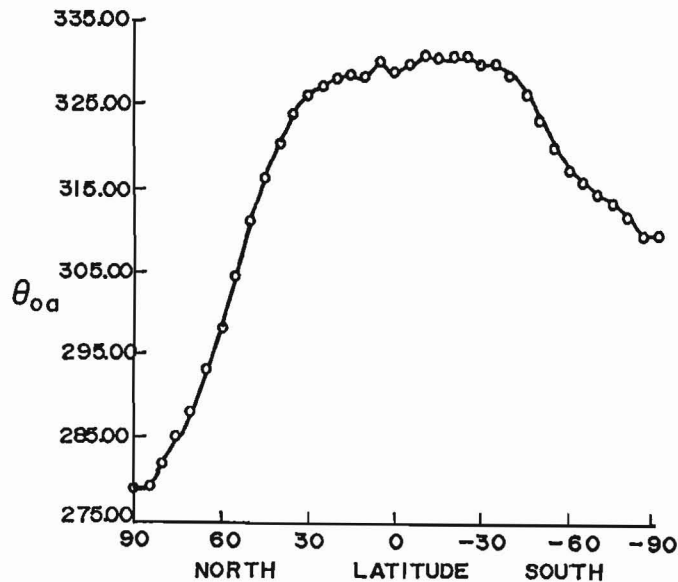


FIG.14 VARIATION OF ATMOSPHERIC POTENTIAL TEMPERATURE WITH LATITUDE (L.P)

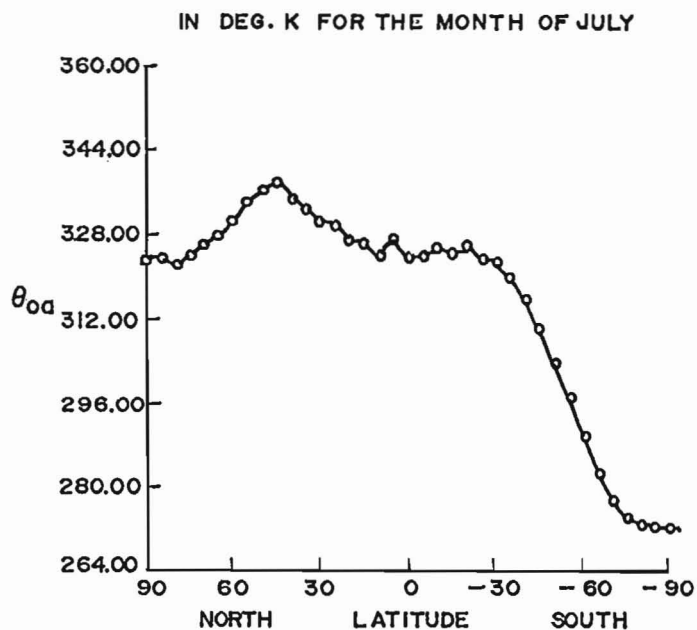


FIG. 15. VARIATION OF ATMOSPHERIC POTENTIAL TEMPERATURE WITH LATITUDE (L.P)

(c) The rainfall maximum shifts from one hemisphere to other with season. The rainfall is maximum at the summer pole because of its greater water availability than at the equator where the soil moisture is low.

(d) The equatorial rainfall maximum migrates during summer up to about 30° towards the summer pole.

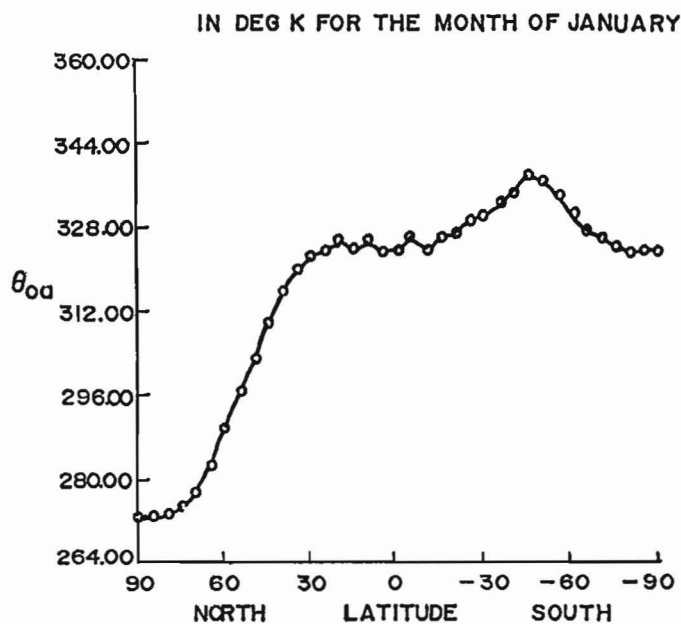


FIG. 16. VARIATION OF ATMOSPHERIC POTENTIAL TEMPERATURE WITH LATITUDE (L.P)

(e) Deserts form in both hemispheres between 35° to 60° . The tropical desert does not form in this experiment mainly due to the migration of the rainfall belt. However, the middle latitude desert is more extended than in the ocean globe experiment.

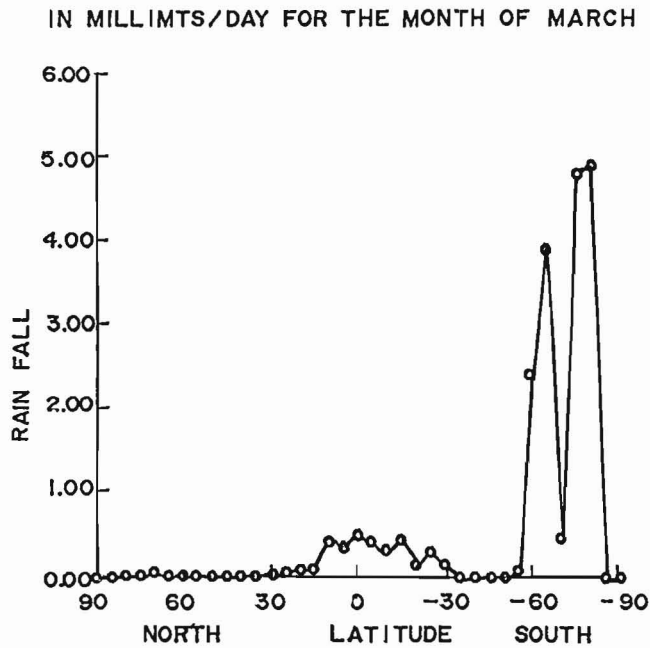


FIG. 17 VARIATION OF RAIN FALL WITH LATITUDE (L.P)

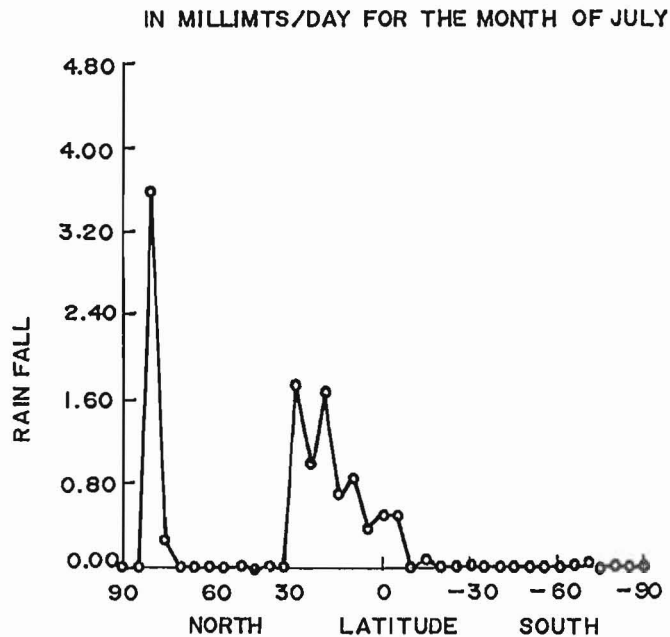


FIG. 18 VARIATION OF RAIN FALL WITH LATITUDE (L.P)

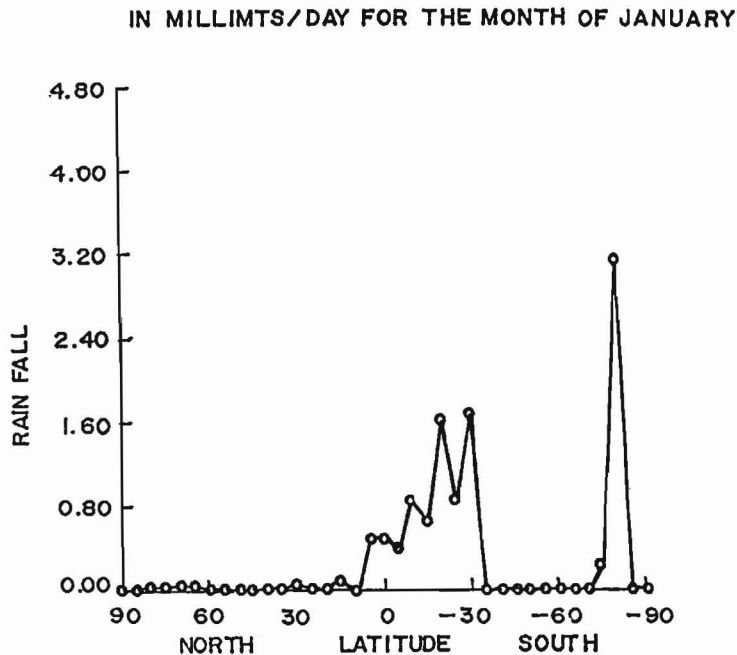


FIG.19. VARIATION OF RAIN FALL WITH LATITUDE (L.P)

5. Some comments

The simple climate models, necessarily, contain parameterization of integrated effects. Otherwise we will end up with a GCM. So these models must be looked upon as phenomenological, hypothesis producing and some times predicting models.

In this model, the very important poloidal motion parameterization depends on a tuning Sellers' parameter b . In our view, this has to be improved by bringing in momentum considerations. The results presented here depend on this single tuning parameter. However Sellers (1973) could get realistic poloidal motions utilizing this parameter, for the present climatic conditions. Hence the results given here may not be expected to be far from reality. Another crucial area is the parameterization of small and large scale precipitation in the model.

6. Conclusions

We arrived to the following main conclusions with these toy model experiments:

- (a) The tropical maximum rain belt migrates very little ($< 5^\circ$) on an ocean globe.
- (b) On a land globe it migrates to about 30° .
- (c) On a global ocean the model gives a tropical desert. The land planet does not have this due to the migration of the rain belt.
- (d) On the ocean globe complete deglaciation takes place in the model. On the land globe ice melts completely in summer and restores in winter from the pole to 60° .

APPENDIX

Notation

p : pressure

ϕ : latitude

t : time

D : any dependent variable

D_o : zonal mean of D

$\overline{\overline{D}}_o$: zonal and vertical mean of D

$\overline{\theta}_{oa}$: zonal mean potential temperature of the atmosphere

a : suffix to indicate atmosphere

a : radius of the Earth

ϵ_{oa} : zonal mean mixing ratio of the atmosphere

v_{oa} : zonal mean meridional velocity of the atmosphere

Coefficient of large scale eddy heat conduction in the atmosphere: $K_{HT} = 0.25 |\Delta T| 10^6 \text{ m}^2/\text{sec}$.

Coefficient of large scale eddy water vapour diffusion in the atmosphere: $K_{H\epsilon} = K_{HT}$

Surface pressure: $p_s = 1000 \text{ mb} = 10^5 \text{ N/m}^2$

s : suffix indicating surface

B : suffix indicating 850 mb level

Mean atmospheric pressure: $p_a = 500 \text{ mb} = 5 \times 10^4 \text{ N/m}^2$

$Q_{oa}^{(1)}$: atmospheric heating due to shortwave radiation

$Q_{oa}^{(2)}$: atmospheric heating due to longwave radiation

$Q_{oa}^{(3)}$: atmospheric heating due to sensible heat flux

$Q_{oa}^{(4)}$: atmospheric heating due to condensation

$H_{os}^{(1)}$: net heat flux at the surface due to shortwave radiation

$H_{os}^{(2)}$: net flux at the surface due to longwave radiation

$H_{os}^{(3)}$: net flux at the surface due to sensible heat transfer

$H_{os}^{(4)}$: net flux at the surface due to latent heat transfer

$H_{os}^{(5)}$: net flux at the surface due to sub-surface heat transfer

Latent heat of evaporation: $L = 2.5 \times 10^6 \text{ Joules/kg}$

ω : vertical velocity in the atmosphere

θ_{ow} : zonal mean ocean temperature

v_{ow} : zonal mean meridional velocity in the ocean

K_{HW} : coefficient of large scale eddy heat conduction in the ocean

w : subscript to indicate ocean water

Depth of the active ocean layer: $h_w = 100$ m

$$\bar{a} = \pi/h_w$$

θ_D : sub-surface temperature taken from Saltzman and Vernekar (1971)

C_j : specific heat of the lower surface material

Mass per unit area of the lower active surface j material: $M_j = \rho_j h_j$

Density of the lower surface ice material: $\rho_{si} = 1000$ kg/m³

Density of the lower surface dry soil: $\rho_{sDs} = 1600$ kg/m³

ρ_{sws} : density of the lower surface wet soil

Density of the lower surface ocean water: $\rho_{sw} = 1000$ kg/m³

ρ_j : density of the surface j material (ice, land or water)

h_j : active depth of the surface j material

$\epsilon_o^*(p)$: saturation humidity mixing ratio at level p

ϵ_{os}^* : saturation humidity at the surface

An empirical constant in eq. (23): $e_2 = 1.27$

An empirical constant in eq. (23): $f_2 = -32.0$ Joules/m²/sec

ev : evaporation

Atmospheric opacity: $\chi = 0.35$ to 0.55

λ_a : atmospheric albedo

λ_s : surface albedo

Steffan-Boltzman constant: $\sigma = 5.67 \times 10^{-8}$ Joules/m²/sec/^oK⁴

Downward longwave emissivity of the atmosphere: $\nu_1 = 1.2$

Upward longwave emissivity of the atmosphere: $\nu_2 = 0.8$

Surface emissivity: $\Gamma = 0.95$

$\bar{\chi}_j$: an empirical sub-surface conductivity parameter for surface j material

$$\bar{\chi}_j = \chi_j^*/h_j$$

χ_j^* : a gross coefficient of conductivity for surface j material

$\bar{\chi}_{si} = \bar{\chi}_j$ for ice

$\bar{\chi}_{sDs} = \bar{\chi}_j$ for dry soil

An empirical constant in eq. (28): $a_1 = 0.70$

An empirical constant in eq. (29): $C_o = 0.76$

C'_1 : an empirical constant in eq. (29)

G_o : downward longwave radiation for clear skies from the atmosphere

G_{on} : downward longwave radiation for cloudy skies from the atmosphere

B_o : upward longwave radiation from the surface for clear skies

R_f : rainfall

R_{f1} : large scale rainfall

R_{f2} : small scale convective rainfall

R_o : solar constant

P^o : porosity

Active moisture depth of the dry soil: $H_d = 1$ m

\bar{w} : water availability

S_m : soil moisture

e : void ratio

Specific heat of dry soil: $C_{sDs} = 800$ Jules/kg/ o K

Specific heat of water: $C_{sw} = 4200$ Jules/kg/ o K

Specific heat of ice: $C_{si} = 2000$ Jules/kg/ o K

C_{sws} : specific heat of the wet soil

Albedo of the surface ice: $\lambda_{si} = 0.5$

Albedo of the surface water: $\lambda_{sw} = 0.06$

Albedo of the surface dry soil: $\lambda_{sDs} = 0.28$

λ_{sws} : albedo of the surface wet soil

\bar{a}_* : an empirical friction constant occurring in eq. (41)

An empirical parameter occurring in eq. (42): b = taken from Sellers

Coriolis parameter $f = 2\Omega \sin \phi$

Angular velocity of the Earth: $\Omega = 7.29 \times 10^{-5}$ /sec

Gas constant for air: $R = 287$ Joules/kg/ o K

REFERENCES

- Held, I. M. and A. Y. Hou, 1980. Non-linear axially symmetric circulation in a nearly inviscid atmosphere. *J. Atmos. Sci.*, **37**, 515-533.
- Kondratyev, K. Ya., 1972. Radiation processes in the atmosphere. World Meteorological Organization No. 309.
- Kubota, I., 1972. Calculation of seasonal variation in the lower troposphere with heat budget equations. *J. Meteor. Soc. Japan*, **50**, 18-26.
- Kurihara, Y., 1971. Seasonal variation of temperature in an atmosphere at rest. *J. Meteor. Soc. Japan*, **49**, 537-544.
- Ramasastry, A. A., De. U. S., D. V. Vaidya and G. Sundari, 1986. Forty day mode and medium range forecasting. *Mousam*, **37**, 305-312.

- Saltzman, B. and A. D. Vernekar, 1971. An equilibrium solution for the axially symmetric component of the Earth's macro climate. *J. Geophys. Res.*, **76**, 1498-1524.
- Sellers, W. D. 1973. A new global climate model. *J. Appl. Meteor.*, **12**, 241-254.
- Sikka, D. R. and S. Gadgil, 1980. On the maximum cloudiness zone and the ITCZ over Indian longitudes during the Southwest monsoon. *Mon. Wea. Rev.*, **108**, 1840-1853.
- Webster, P. J. and I. C. Chow, 1980. Low frequency transition of a simple monsoon system. *J. Atmos. Sci.*, **37**, 368-382.